Normalization of laser-induced breakdown spectroscopy spectra using a plastic optical fiber light collector and acoustic sensor device

Francisco Anabitarte, Luis Rodríguez-Cobo, José-Miguel López-Higuera, and Adolfo Cobo*

Photonics Engineering Group, University of Cantabria, Santander 39005, Spain

*Corresponding author: adolfo.cobo@unican.es

Received 27 June 2012; revised 25 October 2012; accepted 8 November 2012; posted 8 November 2012 (Doc. ID 171500); published 30 November 2012

To estimate the acoustic plasma energy in laser-induced breakdown spectroscopy (LIBS) experiments, a light collecting and acoustic sensing device based on a coil of plastic optical fiber (POF) is proposed. The speckle perturbation induced by the plasma acoustic energy was monitored using a CCD camera placed at the end of a coil of multimode POF and processed with an intraimage contrast ratio method. The results were successfully verified with the acoustic energy measured by a reference microphone. The proposed device is useful for normalizing LIBS spectra, enabling a better estimation of the sample's chemical composition. © 2012 Optical Society of America

OCIS codes: 300.6210, 060.2370, 110.6150.

1. Introduction

Laser-induced breakdown spectroscopy (LIBS) is an atomic emission spectroscopic technique that can detect and quantify analytes in solid, liquid, and gaseous samples. It is based on a high power pulsed laser that ablates a small amount of material, creating a plasma. The light emission from the plasma is captured in the optical range through a spectrometer. From the analysis of the emission lines from the atomic species in the plasma, information about the sample's composition and condition can be inferred [1].

The LIBS technique requires little or no sample preparation, and it is a versatile method that enables in-field applications, such as identification of pigments in paintings, analysis of archeological findings, detection of contaminants in air, water, or soil, or, more recently, geological analysis in space exploration [2,3].

However, it is difficult to perform an accurate quantitative analysis of the sample composition. Laser plasma formation is a nonlinear process, and minor fluctuations in laser beam energy or sample properties can result in a large deviation of atomic line intensity in the spectrum. Among others, chemical and physical matrix effects between the different atomic species [4,5], shot-to-shot fluctuations of the laser pulse parameters (energy, duration, etc.) [6], influence of particles ejected from previous pulses [7], variations in the spatial shape of the plasma plume that affects the light collection efficiency of the spectrometer, and changes in surface conditions of the sample and the experimental setup and its environment in general have been identified as potential sources of errors in the quantitative sample evaluation [8].

Furthermore, laser-induced plasma emission seems to be a chaotic process in the sense that the overall intensity of the resulting optical spectrum is highly dependent on the initial conditions, and significant fluctuations occur even with constant

1559-128X/12/348306-09$15.00/0

parameters and a strict control of the experimental setup. For that reason, several consecutive laser shots are averaged or integrated into a single spectrum. However, this doesn't totally remove signal variability, and the quantitative analysis still can suffer from fluctuations of the laser profile in multimode lasers [9] and, to a lesser extent, laser pulse energy and focusing variations.

In order to mitigate this problem, several techniques like calibration-free LIBS [10] or normalization procedures have been proposed [11]. One simple possibility is so-called internal standardization, already discussed in the very first paper proposing the LIBS technique [12]. This solution is based on the intensity of the emission line of the element to be quantified being divided by the intensity of a weak spectral line of another element whose concentration is known or at least is constant among samples, as this ratio has been found to vary to a much lesser extent than the absolute intensity. However, not all pairs of lines are suitable candidates, as they must satisfy certain spectroscopic criteria: pairs with similar excitation potential, intensity differences smaller than 10 times, and spectral proximity have provided good results [11]. Therefore, depending on the sample, it is not always possible to find suitable lines for this internal standardization within the captured spectral range.

External standardization, on the other hand, is based on the use of an external signal derived from the ablation process as the reference for normalization. One possibility is the acoustic wave generated by the plasma, as the laser pulse produces rapid vaporization of the material surface, and the expansion of the ablated vapor into the surrounding gas forms a shockwave that generates a sound. Although some works have found a complex relationship between the vaporized mass and the laser irradiance for large irradiance values due to the plasma shield effect [13], it is generally assumed that the intensity of the acoustic wave is linearly related to the laser irradiance, and therefore, it is a valid signal for normalization purposes [4,11,14,15]. Acoustic emission is usually detected with standard microphones in the human acoustic detection range, allowing measurement of the acoustic signal from distances up to several meters from the target.

In this paper, the use of a bare polymer optical fiber is proposed as an acoustic sensor for normalization purposes, based on the sensing principle of speckle interferometry [16]. This effect is extremely sensitive to mechanical perturbations of the optical fiber and has the potential to surpass the performance of conventional microphones. However, the attainable sensitivity is much dependent on the acoustic–mechanical behavior of the optical fiber and on the algorithm that processes the speckle pattern to obtain the acoustic signal. The proposed optical fiber, coiled around the point of plasma formation, also acts as the light capturing element for the spectrometer. Plasma emission is usually collected by means of a large-core silica optical fiber coupled with a lens system pointed to the zone where the plasma plume is expected to be [17,18]. This is an efficient system that captures a maximum amount of light from the plasma, but it is difficult to align and its efficiency suffers from fluctuations in the spatial position and shape of the plasma plume [19]. Other approaches that provide spatial integration, such as coaxial capturing through pierce mirrors, add some complexity to the setup [20]. Instead, in the proposed approach, the light is captured through the fiber's cladding on the inner part of the coil and propagated within the core to the spectrometer, thus performing a spatial integration of the optical emission that makes the alignment less critical [21]. One additional advantage of the proposed device over standard electromechanical microphones is the intrinsic immunity against electromagnetic interferences and the chemical inertness of the optical fiber, thus allowing its use in harsh or dangerous environments.

In the next section the design of the light capturing and acoustic sensing device is described, while the experiments performed to assess its performance as a light collector and acoustic sensor are reported in Section 3.

2. Device Description

The proposed device is based on a coiled plastic optical fiber (POF) positioned around the plasma emission and above the surface of the material under study by the LIBS setup (Fig. 1). A short length of poly(methyl methacrylate) (PMMA) optical fiber, without any protective coating, and core and cladding diameters of 980 and 1000 μm, respectively, has been coiled with a coil diameter of a few centimeters. The light from a He–Ne laser is inserted into one end of the fiber, while the other end is split into two optical outputs using a bifurcated fiber. One of the output fibers is connected to a spectrometer to obtain the spectrum from the plasma emission, while the other is connected to a conventional video camera to visualize the speckle pattern created over the CCD surface. An optical bandpass filter, centered at the He–Ne laser wavelength, is placed between the CCD and the fiber to remove any light contribution from the plasma entering the camera that could interfere with the speckle pattern. Care must be taken also to prevent light from the He–Ne laser from reaching the intensified detector of the spectrometer, but in the reported experiments, the laser wavelength of 632.8 nm is well outside the spectral window of analysis, from 450 to 550 nm. The aim of this configuration is to collect and analyze the plasma emission with the spectrometer and, simultaneously, to record the speckle pattern with the camera to estimate the acoustic emission from the plasma.

Several designs of the coil patterns and sizes were tested: in particular, coils with circular, square, and hexagonal shapes. They were built using a rigid cast of PMMA with the intended shape to coil the POF.

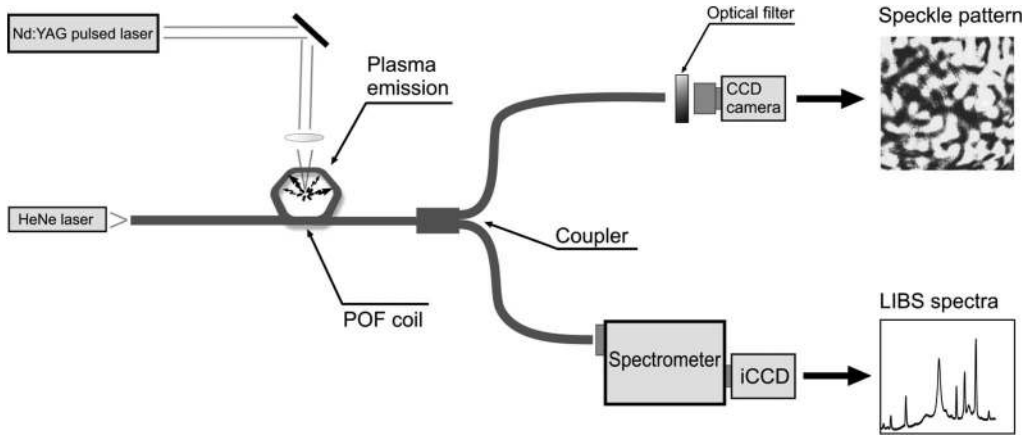

Fig. 1. Sensor device based on a coiled plastic optical fiber (POF) for simultaneously collecting the light emission from the plasma and detecting its acoustic shockwave.

One of the mechanisms that enable the light entering the fiber through the cladding to be collected and guided is the presence of scattering centers in the core–cladding interface due to the manufacturing process [22]. However, the scattering plays a minor role in the capturing efficiency, which is actually boosted by the presence of small-radius curvatures in the coil. Those sharp curvatures allow for the incoming rays of light to fulfill the total internal reflection condition at the core–cladding boundary and to be guided by the fiber. It was found that the hexagonal pattern, with six sharp curvatures per turn, is the most efficient design. It was also found that the number of turns is not critical regarding the light capturing capability, because light captured by a sharp curvature and guided by the optical fiber can also escape at the exterior surface of the next curvature, depending on the incident angle, the exact shape of the coil, and the opto-geometrical parameters of the fiber. Our hypothesis is that the first sharp curvature, the closest to the spectrometer, is the one contributing the most to the overall capturing efficiency. Adding new curvatures (i.e., increasing the number of turns) increases the captured light, but most of it is lost before it reaches the spectrometer. Thus, a single-turn coil has a collecting efficiency similar to a many-turn design.

The influence of the coil diameter was also investigated, and, as expected, small coil diameters have better collecting efficiency. This is mainly due to the dependence of the optical fiber cross section on the square of the distance, as seen by the emitted light from the plasma. However, the coil diameter should be large enough to be safely placed around the plasma plume without the optical fiber being degraded by the high temperatures and ablated material ejected from the sample. For this work, a single-turn hexagonal coil with a diameter of 10 mm has been chosen, as a practical compromise between the efficiency and robustness constraints.

This device design enables the simultaneous measurement of the acoustic emission from the plasma. As the fiber's coil is placed very close to the plasma emission, it is exposed to the pressure waves originating from it. The acoustic waves induce strain changes in the optical fiber, which can be detected with different approaches. In this work, the light from a highly coherent laser is launched into the optical fiber, propagating through the coil, where it is projected over the camera's CCD surface. The induced strain can be easily detected from the perturbation of the speckle pattern captured by the camera. Several processing schemes for the analysis of the speckle images have been proposed as estimators of the physical magnitudes inducing the speckle variation [23]. However, a study of those algorithms in order to find out which one is the most suitable to estimate the shock-wave energy from strain-induced speckle variations in multimode optical fibers has not been previously addressed in the literature. In this work, three processing schemes have been considered: first, the absolute difference between two consecutive frames, i.e., the sum of the intensity value of all pixels from the subtraction image of every two consecutive frames ("differential" processing). Second is "contrast" processing, which is calculated as the variance (square of the standard deviation) of all the pixel values divided by the mean value for each image. And finally, there is the calculation of the moment of inertia of the co-ocurrence matrix derived from the temporal history of the speckle pattern ("MoICO" processing) [24].

The maximum frame rate of the camera can be a serious limitation for shock waves with high-frequency content. For example, differential processing produces an estimation of the acoustic wave limited to frequencies up to half the frame rate, which for conventional cameras can be as low as tens of hertz. In the same way, the "MoICO" scheme needs several consecutive temporal images to generate a single estimation of the degree of speckle variation, and therefore the dynamic discrimination of the induced strain is even more restricted. On the other hand, contrast processing is an intraframe algorithm based on the principle that increasing speckle variations (that is, movement of dark and light spots)

within the integration time of a single acquired frame reduces the contrast of the captured image, so its frequency response is twice that of differential processing. Moreover, the measurement of contrast is an estimator of the source of speckle disturbances (the acoustic pressure applied to the optical fiber) with a higher dynamic range and better linearity to accommodate to different acoustic intensities [23]. Therefore, contrast processing seems more suitable for this particular application.

In the next section, experimental results regarding the light capturing capabilities and acoustic wave estimation of this setup are presented.

3. Experimental Results

A. Light Capturing Performance

The behavior of the proposed design as a plasma light collector has been experimentally tested. A Nd:YAG pulsed laser (Lotis LS-2147), operating at a wavelength of 1064 nm, with 16 ns pulses and energies up to 0.9 J per pulse, was used to generate the plasma plume. The light was captured by an Acton SP-300i spectrometer (150 lines/mm grating with its blaze at 500 nm), coupled to a Princeton Instruments PIMAX-3 gated intensified CCD detector with a gain value of ×40. The capturing window was 40 μs, and the delay between the laser pulse and the spectrum capturing was fixed to 4 μs, a typical value that represents a compromise between the intensity of the atomic emission lines and that of the background. The laser beam was focused onto a plate of a leaded brass alloy used as a target. This material was chosen because there are six intense emission lines from zinc and copper at wavelengths around 500 nm, and if the relative amounts of these elements are known, this target could act as a calibration element for the LIBS setup. In addition, the emission lines of these elements comply with the criteria already described for selecting good pairs of lines for internal normalization purposes.

The plasma emission was collected with the proposed optical fiber coil and with standard collecting optics as a reference for comparison purposes, the latter based on volume lenses and a short silica optical fiber with a 400 μm core diameter. The reference collecting optics has been focused and aligned to maximize the amount of captured light. The POF is an ESKA CK-40 type from Mitsubishi Rayon Co. Ltd., with a minimum attenuation of 0.07 dB/m at the wavelength of 570 nm. The coiled fiber was placed over the brass plate, with one end coupled to a He–Ne laser (wavelength of 632.8 nm and 5 mW power), while the other was attached to a bifurcated optical fiber. One output port of the bifurcated fiber was attached to the spectrometer slit entrance and the other end to the CCD camera. The total length of the fiber arm connected to the spectrometer is 1 m. As the fiber attenuation in the wavelength range around 500 nm is below 0.1 dB/m, the added losses are negligible. The coil was placed 2 mm above the sample's surface. This value has been chosen taking into account previous works [19,25] that analyzed the spatial distribution of the light emission from the plasma plume. The plasma height is typically around 5–10 mm, with a point of maximum emission that evolves in time from the surface up to a distance of a few millimeters in the vertical direction. However, the emission intensity can be considered relatively constant along the vertical axis of the plasma, so the vertical distance from the coil to the sample surface is not a critical issue.

A first experiment has been carried out to compare the spectra captured by both techniques. It is known that the PMMA fiber has a stronger absorption coefficient than the silica, and different absorption peaks due to carbon–hydrogen vibrational overtone modes and OH^- ions in the visible range [26]. In Fig. 2, the captured spectra (single shot) for a pulse energy of the laser of 22 mJ (26 J pump) are shown. This low value of pulse energy, slightly above the threshold for plasma formation, has been selected as a worst-case scenario. A wide entrance slit and a low resolution grating were selected in the spectrometer, in order to analyze a wide spectral range, which explains the larger than usual width of the emission lines. Both captured spectra have been normalized to the maximum value. It can be seen that there are no appreciable differences in the shown wavelength range from 470 to 530 nm, thus validating the proposed optical fiber as a light capturing device. However, it must be noted that PMMA has a strong overall absorption in the UV range, so this device has limited applicability outside the visible range. Specifically, its spectral window for a maximum tolerable attenuation of 3 dB/m has been estimated to extend from 320 to 840 nm. The spectrum using the coiled fiber is noisier due to the fact that the collecting efficiency is lower. From the integration of the intensity of both spectra, the capturing efficiency of the coiled fiber can be calculated as 6% with respect to the volume optics reference setup. However, this low figure is compensated by the fact that

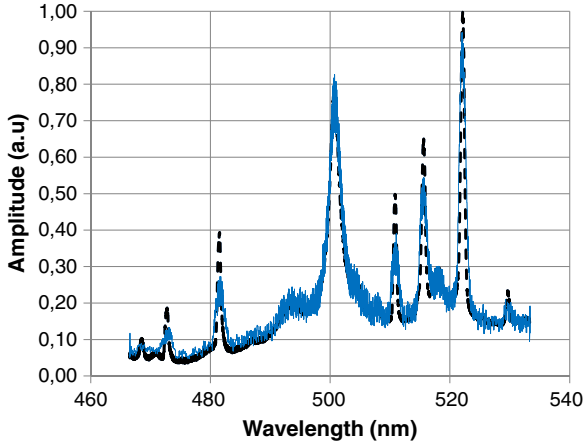

Fig. 2. (Color online) Spectra from the LIBS plasma captured by a standard volume optics setup (dashed curve) and the proposed coiled plastic optical fiber (solid curve).

the alignment is much less critical with this approach. Additionally, the previously mentioned natural variations in the plasma plume's spatial shape in different laser shots greatly affect the capturing efficiency of the volume optics setup, as it is focused on a small spatial point above the target's surface. The spatial integration of the emitted light performed by the coiled fiber reduces this variability.

To analyze how the collecting efficiency of the coiled fiber varies with the position of the coil with respect to the plasma plume, several experiments were carried out. It is expected that light entering the optical fiber at large angles with respect to the normal to the cladding's surface will be better captured and guided, as it can more easily fulfill the total internal reflection condition in the curved fiber. For this reason, the amount of collected light should increase when the coil is not centered on the laser's focal point position. Figure 3 (left) shows the relative capturing efficiency when the center of the fiber coil is shifted in a radial direction from the laser focal point. The light captured by the fiber-optic coil has been measured from the captured spectra at the end of the fiber's arm. For every radial position, the spectra from 30 consecutive laser shots (with constant pulse energy) have been averaged and spectrally integrated to obtain an estimation of the optical power captured and guided by the fiber coil. The measurements have been duplicated and averaged at every spatial point to reduce the error due to the translation stage precision and backslash uncertainty.

As was expected, the capturing efficiency increases for a decentered position, and it doubles for a 3 mm offset, still a safe position with no appreciable fiber degradation due to the generated plasma. This fact can be used to further increase the capturing efficiency if required.

The dependence of the capturing efficiency on the vertical distance from the fiber coil to the sample surface was also investigated, and the result is shown in Fig. 3 (right), with the same experimental conditions as the previous experiment. The reference position of 0 mm is defined with the core axis of the optical fiber at the plane of the sample's surface. It can be seen that the amount of captured light is relatively constant for the lowest vertical positions, with a 50% decrease at a height of 6 mm, which is probably the mean length of the plasma plume. The optimum position to place the coiled fiber, according to the graph, is around 1.5 mm above the sample surface, but this distance is not a critical issue.

B. Acoustic Wave Measurement

The speckle pattern at one end of the optical fiber was analyzed to obtain an indirect measurement of the acoustic energy emitted by the plasma. The optical spectra with the emission lines from the chemical elements in the sample can then be normalized against the estimated energy to reduce the error in the quantitative estimation of the sample composition.

The speckle pattern was created by pointing one output port of the coupler at the CCD surface (without any optics) of a Pixelink PL-A741 camera. Images with 256 levels of gray and sizes of 64×64 pixels were acquired at a frame rate of 510 frames/s. A bandpass optical filter centered at the He–Ne laser wavelength of 632.8 nm was inserted between the optical fiber and the CCD camera, in order to remove any contribution from the emitted plasma that could affect the speckle pattern generated by the He–Ne laser. Although some plasma radiation reaches the CCD through the 10 nm bandpass of the filter, the added noise is negligible: the He–Ne laser optical power at the fiber end is much higher than the background radiation of the plasma in this small spectral window of 10 nm, and the plasma temporal duration of a few microseconds is small compared with the integration time of a camera frame (in the order of a milliseconds). In addition, due to the noncoherent nature of the plasma background, its pattern projected on the CCD is spatially uniform and does not modify the morphological features of the speckle pattern.

For comparison purposes, a conventional moving-coil microphone (HQ Power MICPRO7N) was pointed at the plasma emission at a distance of about 15 cm. Its signal was recorded at a sampling rate of 44,100 Hz with 16 bit resolution. Despite the optical

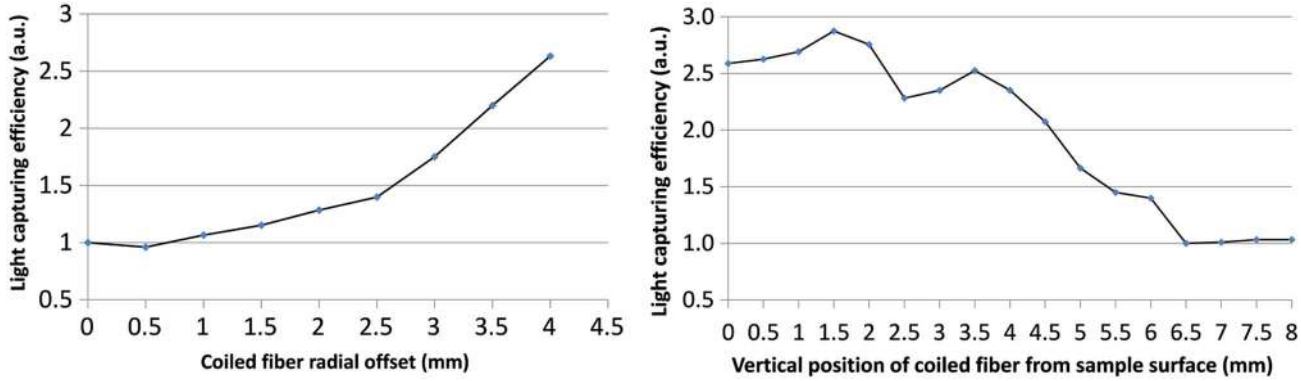

Fig. 3. (Color online) Light capturing efficiency of the coiled plastic optical fiber for different horizontal positions decentered from the plasma plume (left), and for different vertical distances from the sample's surface (right).

fiber coil and the reference microphone being situated at different distances from the plasma emission (a few millimeters versus 150 mm), both sensors are far from the "blast wave region" and within the acoustic domain [27], so they should offer a similar measurement of the acoustic emission.

The plasma emission spectra and the acoustic signals have been recorded at different Nd:YAG laser pump energies from 28 to 37 J in steps of 1 J. In this range, the laser pulse energy ranges from 86 to 345 mJ and is linearly related to the laser pump energy. For every energy setting, 40 laser shots have been delivered to the sample over the same surface point. All the measurements (pulse energy, LIBS spectra, and acoustic energy from the microphone and from the optical fiber's speckle signal) have been averaged for the 40 consecutive shots to obtain a single value for every energy point. Due to this averaging process, which reduces the shot-to-shot variability, it is expected that the intensities of the emission lines and the acoustic energy follow the pulse energy. For this reason, the main performance figure of the proposed speckle-based sensor system is its ability to obtain an estimation of the acoustic signal similar to the one provided by a conventional microphone, and to reduce the variations of the emission lines' intensities at different laser energies using the acoustic signal provided.

The acoustic energy has been estimated using the following procedure: for the microphone, the root-mean-square (RMS) of the acoustic signal has been calculated for every sample and its seven neighbor samples (thus defining a sliding window of eight samples), and the RMS signal is integrated around the peak corresponding to each laser shot to obtain its energy estimation. We consider the temporal width of a peak as the time interval for which the RMS amplitude is above 10% of the maximum value of the peak.

On the other hand, the acoustic energy captured by the fiber coil has been estimated from the speckle signal using the three previously mentioned procedures. The differential processing scheme performs the pixel-by-pixel subtraction of two consecutive speckle images, the energy being estimated as the sum of all the pixel values in the differential image. The contrast processing scheme calculates the ratio between the spatial standard deviation and the mean value of all pixels in every image, the energy estimation being the inverse of this contrast value. Finally, the "MoICO" method first extracts a 1×64 pixel horizontal strip from the center of every image, and the rows are concatenated to form the temporal history of the speckle pattern (THSP). Then a co-ocurrence matrix with eight levels of gray is calculated from a 4×64 sliding matrix (4 pixels in the temporal axis) of the THSP, and the moment of inertia of every co-ocurrence matrix is obtained. The energy estimator with this method is the value of the moment of inertia. For all the methods based on the speckle signal, and due to the relatively low sample rate, a clear maximum of the estimated energy is obtained at the precise time of the laser shot, which is considered to be the acoustic energy emitted by the plasma. It should be noted that these procedures obtain not absolute but relative values of the acoustic energy that cannot be compared with different methods; only the comparison of energy values obtained with the same processing scheme for different laser energies is meaningful.

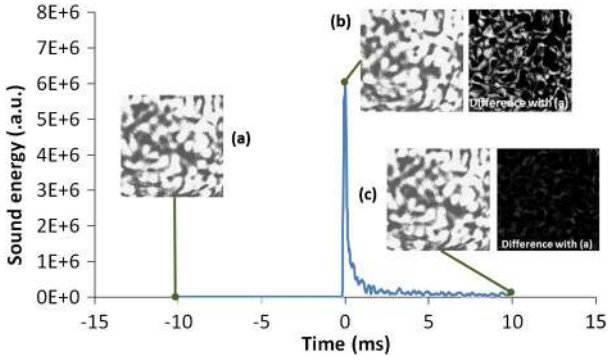

Fig. 4. (Color online) Acoustic pulse from the reference microphone showing the speckle images obtained (a) before, (b) during, and (c) 10 ms after the laser shot.

In Fig. 4, the acoustic energy from the reference microphone is shown for a laser shot of 135 mJ. The speckle images are displayed for illustration purposes before, during, and long after the plasma

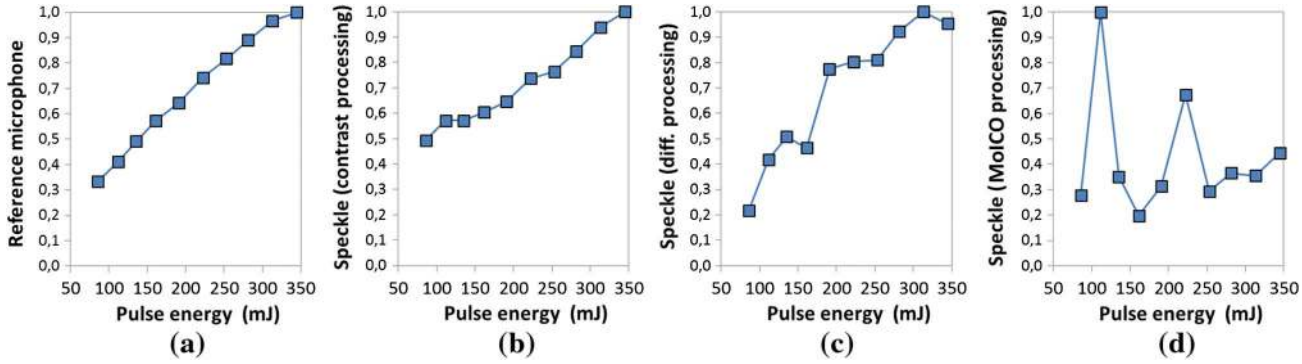

Fig. 5. (Color online) Acoustic energy estimation (a) from the reference microphone from and the speckle pattern analysis using the proposed processing schemes of (b) contrast, (c) differential, and (d) MoICO.

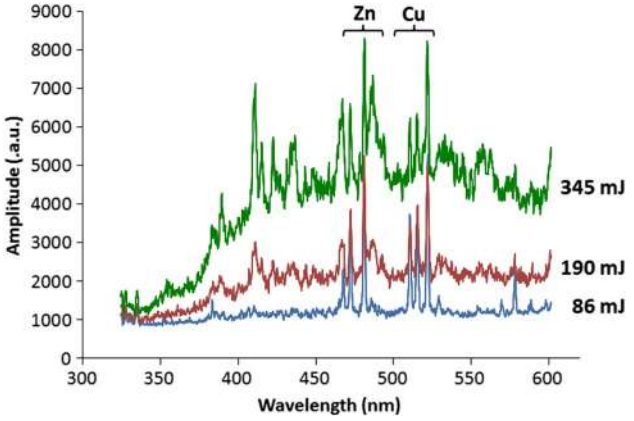

Fig. 6. (Color online) Plasma emission spectra at three different laser energies.

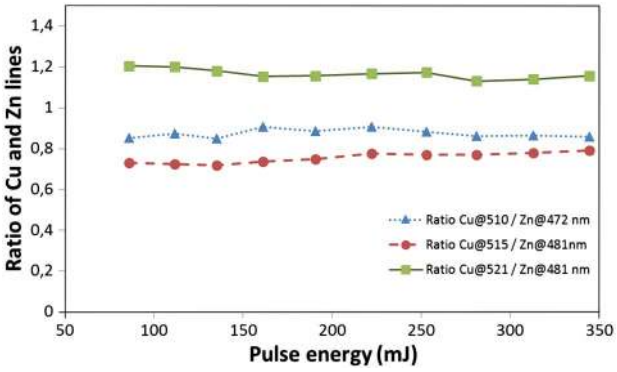

Fig. 7. (Color online) Ratio of three pairs of emission line intensities against the laser pulse energy.

emission. The difference images at the peak maximum and after pulse extinction, with respect to the speckle image at rest, show how the speckle pattern is significantly modified by the shockwave and then returns to its original configuration.

First, the capacity of the acoustic energy, estimated with the proposed method, to follow the pulse energy has been analyzed. Figure 5 shows the dependence of the acoustic energy calculated from the reference microphone, and from the speckle analysis, on the pulse energy. The laser energy sweep corresponds to pump energies from 28 to 37 J (86 to 345 mJ pulse energy, respectively), well above the pump threshold and within the linear range of the Nd:YAG laser. The acoustic energies for each method have been normalized to a maximum value of 1, as they are relative estimations. It can be seen that the microphone has a linear dependence and is able to predict the laser energy delivered to the sample with a correlation value of $R^2 = 0.996$ and a maximum deviation of 3.2%. For the speckle analysis, it can be seen that only the contrast method produces a good linear relationship between the acoustic energy and the laser energy. This method predicted the laser energy variations with a correlation value of $R^2 = 0.97$ and a maximum deviation of 4.3%, values slightly worse than those of the microphone. The sensitivity of the optical fiber detector using this processing scheme is 29% lower. The other speckle processing methods, MoICO in particular, have poor performance in this case. As explained in the introduction, the reason probably is due to the low frame rate of the camera compared with the sound pressure dynamics. A complete shockwave evolution and the corresponding speckle variations are integrated and contained within the temporal period of a single frame. The contrast algorithm is able to obtain the degree of variation of the speckle pattern within that single frame, while the differential scheme requires two consecutive frames, and the MoICO method even more.

The ability of the acoustic signal to improve the accuracy of the composition analysis of the sample at different laser energies has also been explored. In Fig. 6, three LIBS plasma spectra from the leaded brass sample are shown, corresponding to laser energies of 86, 190, and 345 mJ. Six emission lines are visible: three lines of zinc at 468.0, 472.2, and 481.0 nm and three lines of copper at 510.5, 515.3, and 521.8 nm. As the intensity of these lines increases with the increasing laser energy, the spectra must be normalized to obtain an estimation of the sample composition.

One possible method calculates the ratio of intensities of two lines of different elements, in this case, copper and zinc. The plot of two pairs of lines

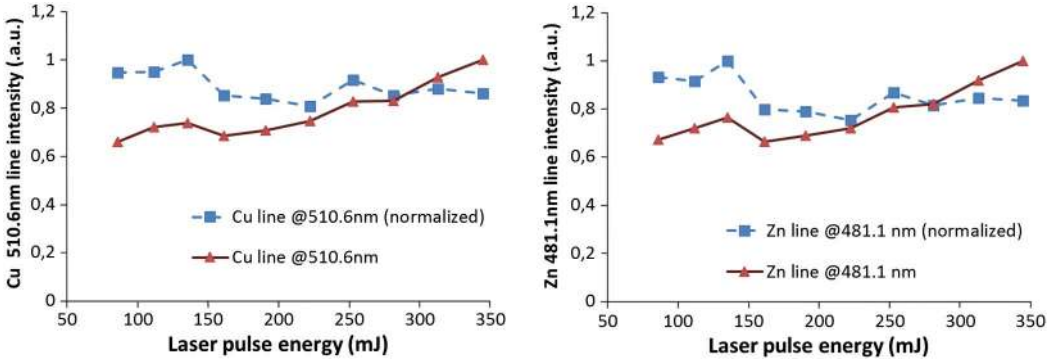

Fig. 8. (Color online) Normalization capability of the acoustic signal (contrast processing of the speckle images) for two emission lines of copper (left) and zinc (right).

against the laser energy, which should be constant as the sample composition does not vary during the experiments (58% copper, 39% zinc, 3% lead), is shown in Fig. 7. The line intensities have been calculated as the integrals of the emission lines. Although some variation still remains, it can be seen that the ratio is fairly constant, despite the 1:4 change in the energy delivered to the sample.

However, depending on sample composition and intended analysis, it is not always possible to find a good line candidate to calculate the ratio. For this reason, the external (i.e., acoustic) normalization can be useful when a suitable line pair of two elements is not available. In Fig. 8, the absolute intensity of the copper emission line at 510.6 nm is plotted against the pump laser energy. It can be seen (left) that the acoustic normalization using the contrast processing of the speckle signal is able to reduce its variation from 33% to 20% for the entire range of energies. In the same way, the unwanted variations of the emission line of zinc at 481.1 nm (right) are reduced from 33% to 24% if the absolute intensity is divided by the acoustic signal. Similar results can be found for other emission lines.

4. Conclusions

A light collector and acoustic POF sensor device useful in the normalization of LIBS spectra is proposed and demonstrated in this paper. The light emitted by the plasma is collected by a POF coil with uncoated cladding and propagated through its core. Its collecting efficiency is 6% of the classical solution of volume optics pointed at the plasma plume; however, in contrast, it is able to integrate the optical emission around the plasma and the alignment is less critical. By de-centering the POF coil around the plasma emission, more light rays fulfill the total internal reflection condition in the core–cladding interface, and hence the efficiency can be tripled.

The acoustic wave is measured by means of the strain-induced perturbation of the speckle pattern at the fiber's end when light from a He–Ne laser is transmitted through the coil. The speckle images have been captured by a conventional CCD camera. Several processing schemes of the images have been tested in order to obtain an estimation of the acoustic wave that has been compared with a reference conventional microphone. It has been found that the calculation of the intraimage contrast ratio offers the best estimation of the acoustic energy. It has been demonstrated that using the measured acoustic wave, the optical spectra of the atomic emission from the sample in the LIBS setup can be normalized against unwanted changes in the experimental conditions, such as the laser pulse energy. This normalization can enable a better estimation of the sample's chemical composition.

Future works will try to study in more detail the influence of fiber-optic geometrical parameters (such as coil diameter or distance to the sample) on the capturing efficiency and sensitivity to the acoustic wave, as well as the effect of the gate delay on the performance of the acoustic normalization.

This work was supported in part by the Science and Technology Ministry of the Spanish Government through the TEC2010-20224-C02-02 and FIS2010-19860 projects and grants AP2007-02230 and AP2009-1403.

References

1. D. A. Cremers and L. J. Radziemski, *Handbook of Laser-Induced Breakdown Spectroscopy* (Wiley, 2006).
2. R. Gaudiuso, M. Dell'Aglio, O. de Pascale, G. S. Senesi, and A. de Giacomo, "Laser induced breakdown spectroscopy for elemental analysis in environmental, cultural heritage and space applications: a review of methods and results," Sensors **10**, 7434–7468 (2010).
3. D. W. Hahn and N. Omenetto, "Laser-induced breakdown spectroscopy (LIBS), part II: review of instrumental and methodological approaches to material analysis and applications to different fields," Appl. Spectrosc. **66**, 347–419 (2012).
4. C. Chaleard, P. Mauchien, N. Andre, J. L. Uebbing, Lacour, and C. Geertsen, "Correction of matrix effects in quantitative elemental analysis with laser ablation optical emission spectrometry," J. Anal. At. Spectrom. **12**, 183–188 (1997).
5. F. R. Doucet, T. F. Belliveau, J. L. Fortier, and J. Hubert, "Use of chemometrics and laser-induced breakdown spectroscopy for quantitative analysis of major and minor elements in aluminum alloys," Appl. Spectrosc. **61**, 327–332 (2007).
6. B. C. Castle, K. Talabardon, B. W. Smith, and J. D. Winefordner, "Variables influencing the precision of laser-induced breakdown spectroscopy measurements," Appl. Spectrosc. **52**, 649–657 (1998).
7. H. Lindner, K. H. Loper, D. W. Hahn, and K. Niemax, "The influence of laser-particle interaction in laser induced breakdown spectroscopy and laser ablation inductively coupled plasma spectrometry," Spectrochim. Acta B: At. Spectrosc. **66**, 179–185 (2011).
8. E. Tognoni, G. Cristoforetti, S. Legnaioli, V. Palleschi, A. Salvetti, M. Mueller, U. Panne, and I. Gornushkin, "A numerical study of expected accuracy and precision in calibration-free laser-induced breakdown spectroscopy in the assumption of ideal analytical plasma," Spectrochim. Acta B: At. Spectrosc. **62**, 1287–1302 (2007).
9. V. Lednev, S. M. Pershin, and A. F. Bunkin, "Laser beam profile influence on LIBS analytical capabilities: single vs. multimode beam," J. Anal. At. Spectrom. **25**, 1745–1757 (2010).
10. E. Tognoni, G. Cristoforetti, S. Legnaioli, and V. Palleschi, "Calibration-free laser-induced breakdown spectroscopy: state of the art," Spectrochim. Acta B: At. Spectrosc. **65**, 1–14 (2010).
11. N. B. Zorov, A. A. Gorbatenko, T. A. Labutin, and A. M. Popov, "A review of normalization techniques in analytical atomic spectrometry with laser sampling: from single to multivariate correction," Spectrochim. Acta B: At. Spectrosc. **65**, 642–657 (2010).
12. E. F. Runge, R. W. Minck, and F. R. Bryan, "Spectrochemical analysis using a pulsed laser source," Spectrochim. Acta **20**, 733–736 (1964).
13. S. Palanco and J. Laserna, "Spectral analysis of the acoustic emission of laser-produced plasmas," Appl. Opt. **42**, 6078–6084 (2003).
14. A. Hrdlička, L. Zaorálková, M. Galiová, T. Čtvrtníčková, V. Kanický, V. Otruba, K. Novotný, P. Krásenský, J. Kaiser, R. Malina, and K. Páleníková, "Correlation of acoustic and optical emission signals produced at 1064 and 532 nm laser-induced breakdown spectroscopy (LIBS) of glazed wall tiles," Spectrochim. Acta B: At. Spectrosc. **64**, 74–78 (2009).
15. S. Conesa, S. Palanco, and J. J. Laserna, "Acoustic and optical emission during laser-induced plasma formation," Spectrochim. Acta B: At. Spectrosc. **59**, 1395–1401 (2004).

16. W. B. Spillman, Jr., B. R. Kline, L. B. Maurice, and P. L. Fuhr, "Statistical-mode sensor for fiber optic vibration sensing uses," Appl. Opt. **28**, 3166–3176 (1989).
17. A. Hrdlicka, L. Prokes, A. Stanková, K. Novotný, A. Vitesníková, V. Kanický, V. Otruba, J. Kaiser, J. Novotný, R. Malina, and K. Páleníková, "Development of a remote laser-induced breakdown spectroscopy system for investigation of calcified tissue samples," Appl. Opt. **49**, C16–C20 (2010).
18. C. Bohling, D. Scheel, K. Hohmann, W. Schade, M. Reuter, and G. Holl, "Fiber-optic laser sensor for mine detection and verification," Appl. Opt. **45**, 3817–3825 (2006).
19. M. Corsi, G. Cristoforetti, M. Giuffrida, M. Hidalgo, S. Legnaioli, V. Palleschi, A. Salvetti, E. Tognoni, and C. Vallebona, "Three-dimensional analysis of laser induced plasmas in single and double pulse configuration," Spectrochimic Acta B: At. Spectrosc. **59**, 723–735 (2004).
20. P. B. Dixon and D. W. Hahn, "Feasibility of detection and identification of individual bioaerosols using laser-induced breakdown spectroscopy," Anal. Chem. **77**, 631–638 (2005).
21. F. Anabitarte, L. Rodriguez-Cobo, M. Lomer, J. Mirapeix, J. M. Lopez-Higuera, and A. Cobo, "Laser induced breakdown spectroscopy light collector based on coiled plastic optical fiber," in *Proceedings of the 20th International Conference on Plastic Optical Fibers*, Bilbao, Spain, 14 September 2011 (International Cooperative of Plastic Optical Fiber, 2011), pp. 315–319.
22. G. Aldabaldetreku, I. Bikandi, M. A. Illarramendi, G. Durana, and J. Zubia, "A comprehensive analysis of scattering in polymer optical fibers," Opt. Express **18**, 24536–24555 (2010).
23. G. Hernán Sendra, "Activity analysis on dynamic speckle patterns (Análisis de actividad en patrones de speckle dinámico)," Ph.D. thesis (Universidad Nacional de Mar de Plata, 2009).
24. R. Arizaga, M. Trivi, and H. Rabal, "Speckle time evolution characterization by the cooccurrence matrix analysis," Opt. Laser Technol. **31**, 163–169 (1999).
25. J. A. Aguilera, J. Bengoechea, and C. Aragón, "Spatial characterization of laser induced plasmas obtained in air and argon with different laser focusing distances," Spectrochim. Acta B: At. Spectrosc. **59**, 461–469 (2004).
26. C. Koeppen, R. F. Shi, W. D. Chen, and A. F. Garito, "Properties of plastic optical fibers," J. Opt. Soc. Am. B **15**, 727–739 (1998).
27. C. Stauter, P. Gerard, J. Fontaine, and T. Engel, "Laser ablation acoustical monitoring," in *Symposium H on Laser Processing of Surfaces and Thin Films of the 1996 E-MRS Spring Conference, Amsterdam* (Elsevier, 1997), pp. 174–178.